doi:10.1016/j.jmb.2010.10.051 J. Mol. Biol. (2011) 405, 298–314

Contents lists available at www.sciencedirect.com

Journal of Molecular Biology

journal homepage: http://ees.elsevier.com.jmb

PDZ Binding to the BAR Domain of PICK1 is Elucidated by Coarse-grained Molecular Dynamics

Yi He[1], Adam Liwo[1,2], Harel Weinstein[3] and Harold A. Scheraga[1]*

[1]*Baker Laboratory of Chemistry and Chemical Biology, Cornell University, Ithaca, New York 14853-1301, USA*
[2]*Faculty of Chemistry, University of Gdansk, Sobieskiego 18, 80-952 Gdansk, Poland*
[3]*Department of Physiology and Biophysics, Weill Cornell Medical College, Cornell University, 1300 York Avenue, New York, NY 10065, USA*

Received 29 July 2010; received in revised form 22 October 2010; accepted 27 October 2010
Available online 2 November 2010

Edited by D. Case

Keywords:
PICK1;
binding;
hydrophobic interactions;
UNRES force field;
molecular dynamics

A key regulator of α-amino-3-hydroxy-5-methylisoxazole-4-propionic acid (AMPA) receptor traffic, PICK1 is known to interact with over 40 other proteins, including receptors, transporters and ionic channels, and to be active mostly as a homodimer. The current lack of a complete PICK1 structure determined at atomic resolution hinders the elucidation of its functional mechanisms. Here, we identify interactions between the component PDZ and BAR domains of PICK1 by calculating possible binding sites for the PDZ domain of PICK1 (PICK1-PDZ) to the homology-modeled, crescent-shaped dimer of the PICK1-BAR domain using multiplexed replica-exchange molecular dynamics (MREMD) and canonical molecular dynamics simulations with the coarse-grained UNRES force field. The MREMD results show that the preferred binding site for the single PDZ domain is the concave cavity of the BAR dimer. A second possible binding site is near the N-terminus of the BAR domain that is linked directly to the PDZ domain. Subsequent short canonical molecular dynamics simulations used to determine how the PICK1-PDZ domain moves to the preferred binding site on the BAR domain of PICK1 revealed that initial hydrophobic interactions drive the progress of the simulated binding. Thus, the concave face of the BAR dimer accommodates the PDZ domain first by weak hydrophobic interactions and then the PDZ domain slides to the center of the concave face, where more favorable hydrophobic interactions take over.

Introduction

Protein interacting with C kinase 1 (PICK1) is a multi-domain mammalian membrane protein.[1] Its monomeric form contains one post-synaptic density-95/discs large/zonula occludens-1 (PDZ)[2,3] and one Bin/Ampiphysin/Rvs (BAR)[4] domain. Although PDZ and BAR domains are common protein-function domains, PICK1 is the only protein that contains both a PDZ and a BAR domain, and interacts with over 40 proteins in the cell, including receptors, transporters and ionic channels.[5–26] The proteins that interact with PICK1 are involved in different functions ranging from protein phosphorylation to neurotransmission and cell adhesion. The

*Corresponding author. E-mail address: has5@cornell.edu.

Abbreviations used: PICK1, protein interacting with C kinase 1; PDZ, post-synaptic density-95/discs large/zonula occludens-1; BAR, Bin/Ampiphysin/Rvs; AMPA, α-amino-3-hydroxy-5-methylisoxazole-4-propionic acid; LTD, long-term depression; PKCα, protein kinase C alpha; MREMD, multiplexed replica-exchange molecular dynamics; MD, molecular dynamics; UNRES, united residue; PX, phox.

interaction between PICK1 and α-amino-3-hydroxy-5-methylisoxazole-4-propionic acid (AMPA) receptors is essential for induction of synaptic long-term depression (LTD)[27,28] as well as for a new form of cerebellar synaptic plasticity termed calcium-permeable AMPA receptor plasticity. Recent findings also identify an important role for PICK1 in the neuroendocrine system both in insects and vertebrates.[29]

PICK1 is believed to perform its biological function by regulating the trafficking of its binding partners[30–32] or by using protein kinase C alpha (PKCα) to facilitate their phosphorylation.[33–35] The interplay between the two main structural domains of PICK1, the PDZ and BAR domains, depends on the dynamics of the tertiary structure of the protein that involves the flexible connecting loops and termini, especially because the biological function of the protein appears to depend on its dimerization.

The structure of the PDZ domain of PICK1 was determined recently,[36] but the structure of the PICK1-BAR domain is still unknown; notably, however, PICK1-BAR has a high degree of sequence similarity to the Arfaptin and Endophilin BAR domains, whose structures are known.[37,38] Besides this sequence similarity, the PICK1-BAR domain is known to dimerize[34] and is considered to adopt a banana-like shape whose concave surface carries positively charged regions, like the two structurally known proteins. The concave surface of the BAR dimer can act as a curvature sensor that interacts preferentially with curved lipid membranes containing negatively charged lipids.[39–42] Based on this information, Han and Weinstein used homology-modeling and docking methods to build the model of the PICK1 dimer shown in Fig. 1.[43] The linkers (orange and purple) between the PDZ and BAR domains are shown only to complete the protein structure, but the structures of the flexible linker regions are not known.

The model of the PICK1 dimer structure shown in Fig. 1 illustrates the main hypothesis for the regulation of the PICK1 protein by auto-inhibition/disinhibition. Thus, the occlusion of the concave face of the BAR dimer, which is considered to interact with membranes, by the interacting PDZ domains of PICK1, as indicated in Fig 1, has been proposed as the regulatory mechanism for BAR domain function, in which the auto-inhibited complex is activated by the dissociation of the PDZ domains from the BAR surface following their own interaction with the C-termini of specific membrane proteins[40] or proximity to the membrane.[44]

Given the lack of detailed structural information about the complete PICK1 and its putative dimer, it becomes necessary to evaluate the proposed complex with computational-modeling. Because PICK1 is the only protein that contains both a PDZ domain and a BAR domain, making it impossible to employ homology-modeling to determine their modes of interaction, the structural and energetic feasibility of the putative auto-inhibited form of PICK1, and the manner in which the PICK1-PDZ domain finds its way to the binding sites on the crescent-shaped PICK1-BAR dimer, was explored here with restrained multiplexed replica-exchange molecular dynamics (MREMD) and canonical molecular dynamics (MD). The simulations to determine the binding mode of the PICK1-PDZ domain on the BAR dimer surface were started by placing the PICK1-PDZ domain somewhere near the crescent homology-modeled PICK1-BAR domains, and were carried out starting from different initial positions for the PICK1-PDZ domain near the PICK1-BAR domains. The physics-

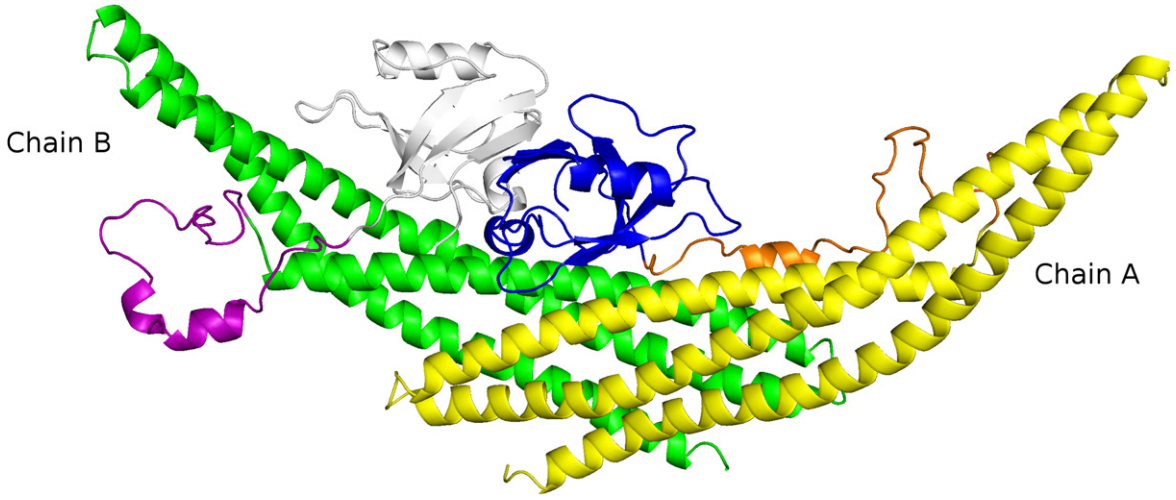

Fig. 1. Homology-modeled structure of the PICK1 dimer from Ref. 43. Chain A consists of the PDZ domain (blue), the linker (orange) and the BAR domain (yellow). Chain B consists of the PDZ domain (gray), the linker (purple) and the BAR domain (green).

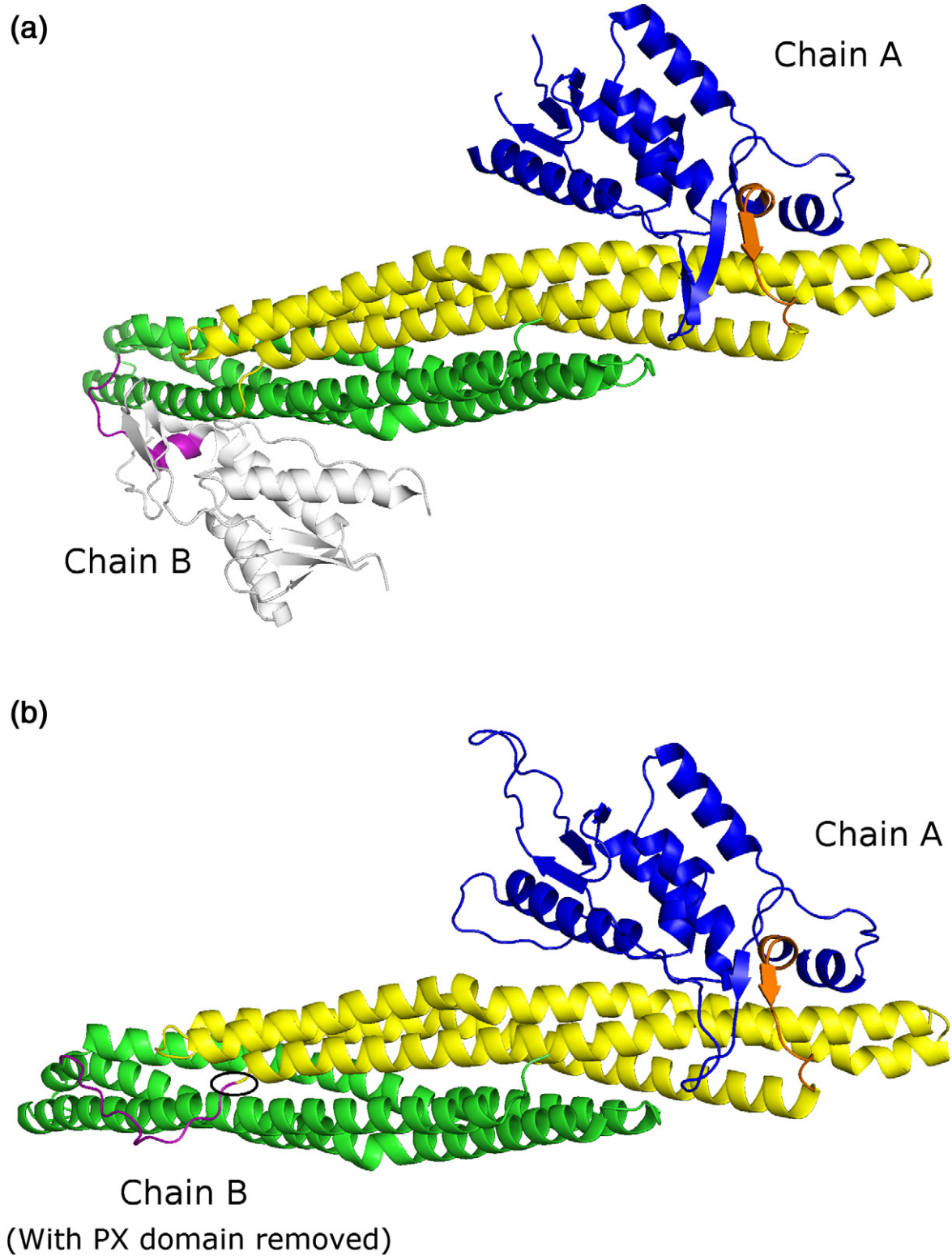

Fig. 2. (a) Experimental structure of the SN9 dimer determined by X-ray diffraction.[64] Chain A consists of the PX domain (blue), the linker (orange) and the BAR domain (yellow). Chain B consists of the PX domain (grey), the linker (purple) and the BAR domain (green). (b) The artificial structure, termed dual-BAR construct of SN9, was built for UNRES simulation based on the experimental structure. In the dual-BAR construct of SN9, the PX domain (gray) was removed from the BAR domain of chain B, and the linker sequence of chain B was used to connect the BAR domains of chains A and B; the connection is marked by a small black ellipse (b).

based united residue (UNRES) force field for off-lattice protein structure simulations was used to facilitate the long computational explorations of the large PDZ/BAR complex system.[45–63] We show here that the preferred binding site on the BAR domain is similar to that found by Han and Weinstein,[43] and that hydrophobic interactions are the dominant stabilization forces, with the large convex face of the BAR dimer attracting the PDZ domain that slides to the central binding pocket where it forms the most favorable hydrophobic interactions.

The reliability of the novel application of the UNRES force field to compute the binding between different large domains within the PICK1 protein is tested here first with cognate simulations for the known structure of Sorting Nexin 9 (SN9, PDB id: 2RAI),[64] a protein that includes a phox (PX) domain and a BAR domain. As in PICK1, the SN9-BAR domain is known to dimerize, as shown in Fig. 2a. Compared to other coarse-grained approaches to model polypeptide chains, which are largely knowledge-based, UNRES is a physics-based force field, using a cluster-cumulant expansion of the effective free energy of a protein plus the surrounding solvent.[49,65] Recently, temperature dependence was included in UNRES[61] to complete its free-energy function character, and the force field was reparameterized based on a global search of the parameter space.[62] To treat proteins containing over 500 amino acid residues, the energy and force calculations were parallelized.[63] The new force field has been shown to perform well in simulations of medium to large proteins containing α, β and α+β structures,[62] and is shown here to produce excellent

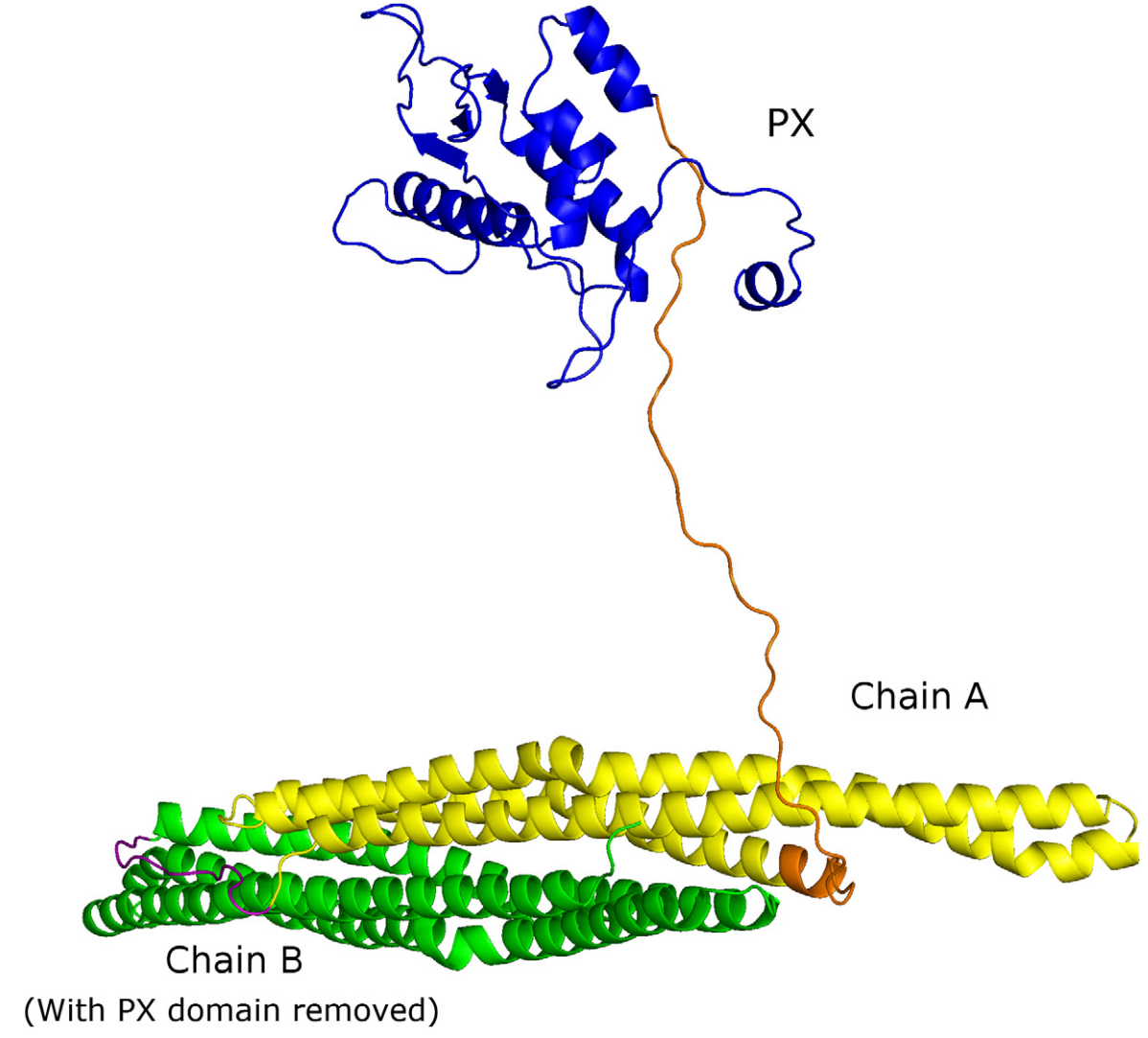

Fig. 3. Structure of the SN9 dual-BAR construct with the PX domain (blue) pulled away from the BAR domains. A 40 residue linker (orange) was produced artificially and built with Modeller.[66–69] The structure shown here was the initial conformation for the subsequent UNRES optimization.

results for the known structure of SN9. Therefore, the same procedure was applied to study the model for the auto-inhibition of PICK1.

Results

The present version of the UNRES force field[62] has been tested on 13 proteins with α, β and α+β structures; however, all of them are single-domain proteins. Therefore, before the work on PICK1 was started, the UNRES force field was explored for its ability to pack the domains of the SN9 dual-BAR construct, which contains a PX domain and two BAR domains, in accordance with the structure determined from X-ray crystallography.[64] The binding of the SN9-PX and SN9-BAR domains and the computed structure of the linker were determined by fixing the conformation and location of the BAR domains and varying the position of the PX domain.

Test MREMD simulations with SN9

Because the focus is the binding of the PX to the BAR domain in the SN9 dual-BAR monomer, the internal geometries of the PX and BAR domains were restrained; however, no restraint was applied to the 40 residue "linker region"[66–69] between the PX and BAR domains. The initial structure for MREMD simulation is shown in Fig. 3. Each trajectory was run for a total of 8×10^6 steps. The set of conformations obtained in the last 8×10^4 steps of each trajectory was analyzed for the presence of native-like conformations.

The C^α rmsd distribution of the MREMD simulation results compared to the "native" structure of the SN9 dual-BAR monomer (shown in Fig. 2b and based on the X-ray structure illustrated in Fig. 2a) is shown in Fig. 4a. A maximum is centered at C^α rmsd 2.5 Å from the native structure. The resulting structures were also subjected to a cluster analysis (with the single-linkage method[70] and an rmsd cutoff of 1.5 Å), and the representative structure of the largest cluster is shown in Fig. 4b compared to the native structure shown in Fig. 4c. These results indicate that the SN9 dual-BAR monomer exhibits a native-like binding pattern of the PX and BAR domains, except for some differences in the 40 residue linker region, showing that the UNRES-based calculations reproduce the correct binding between the PX and dual BAR domains when the distant PX domain is allowed to relax back to its preferred position near the BAR domain. This procedure was then applied to PICK1.

Simulations of PICK1

Simulated binding of the PDZ to the BAR domains of PICK1 by MREMD

Simulations of PICK1 were started from the initial structures shown in Fig. 5. As shown there, two

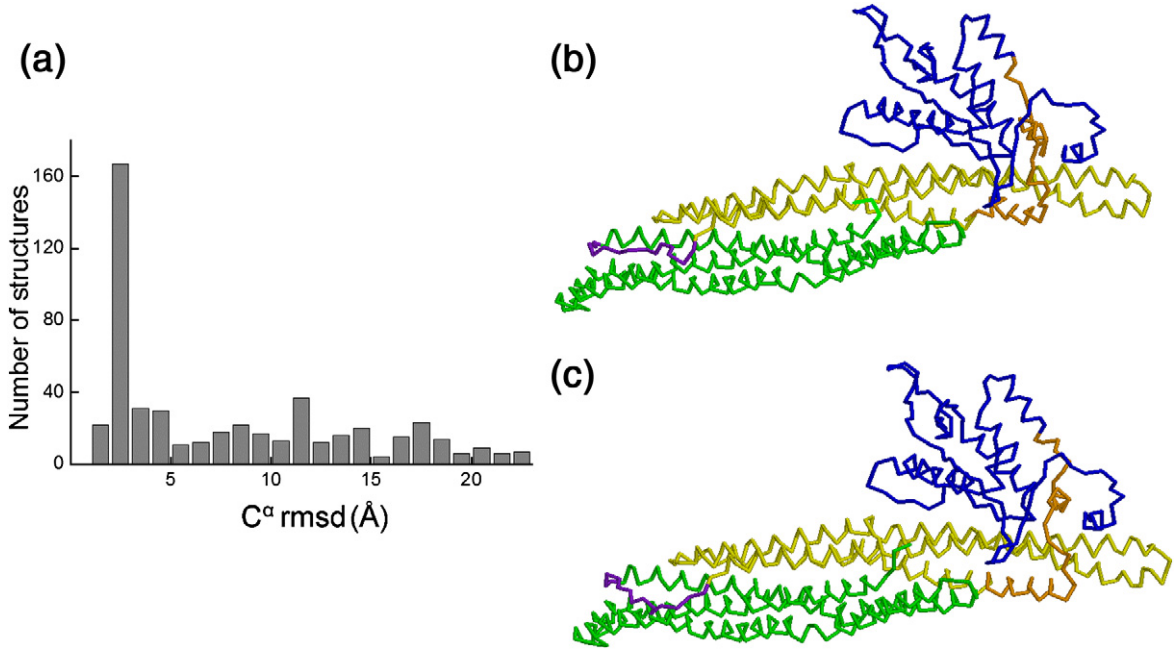

Fig. 4. (a) Distribution of C^α rmsd from the native structure of the dual-BAR construct of SN9. (b) Lowest C^α rmsd structure of the conformations of the dominant cluster of the SN9 dual-BAR construct obtained in UNRES/MREMD simulations. (c) The artificial structure, termed dual-BAR construct of SN9, built for UNRES simulation based on the experimental structure.

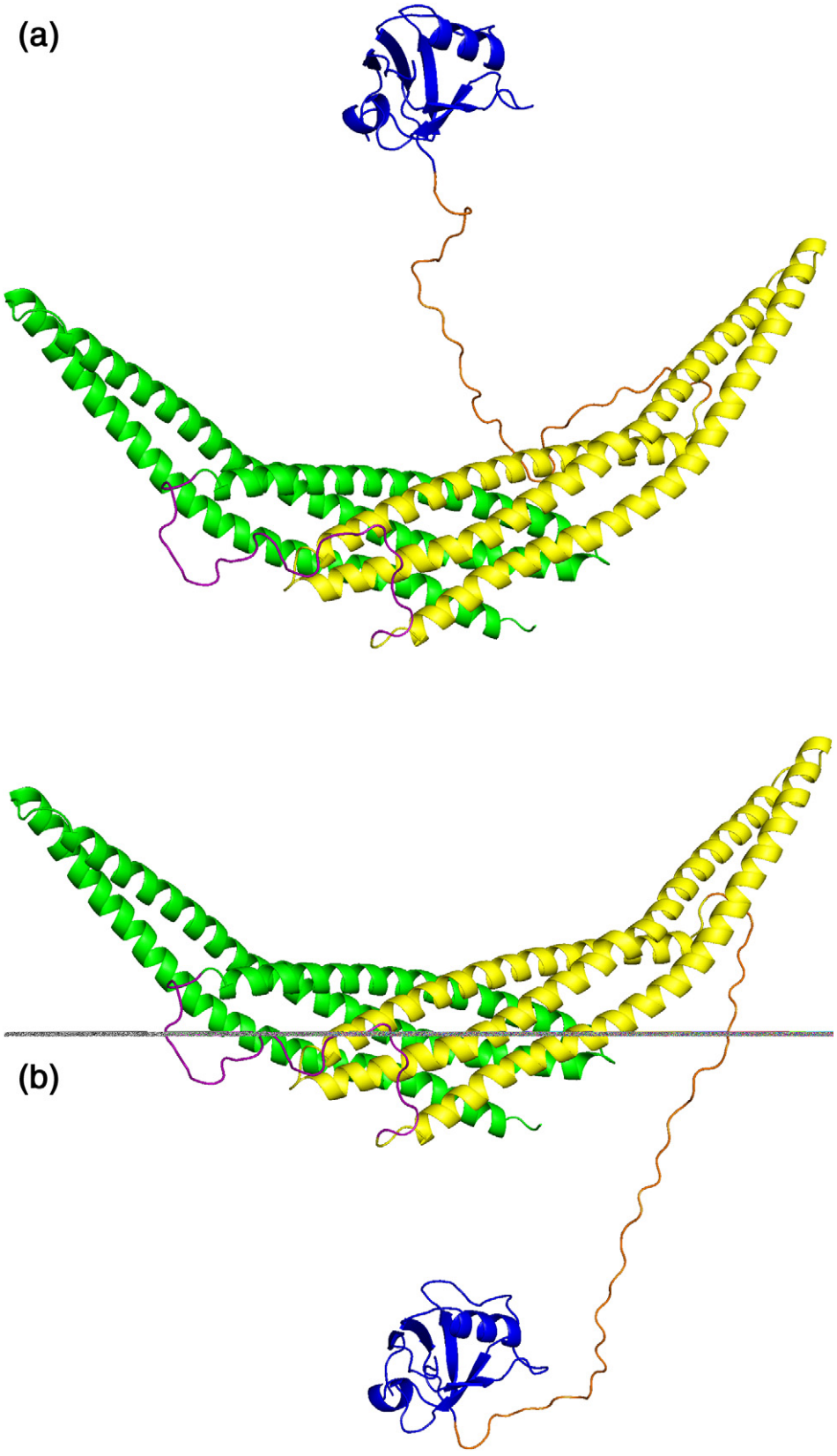

Fig. 5. Initial structures with the PDZ domain pulled away from the BAR domains, selected for subsequent UNRES simulations of the PICK1 dual-BAR construct (built with Modeller).[66–69]

positions were chosen for placing the PDZ domain with respect to the BAR domains, one on the top of the concave face of the BAR domains, as shown in Fig. 5a, and another on the opposite side of the BAR domains, as shown in Fig. 5b. A total of 1×10^7 MD steps were run with MREMD for both initial structures. The set of conformations obtained in the last 8×10^4 steps of each trajectory were analyzed for possible native-like conformations.

To identify the most likely complexes between the interacting domains we parsed the resulting complexes with the single-linkage method[70] of clustering and a C^{α} rmsd cut-off of 2.0 Å. The cluster distributions from simulations, starting with the structures of Fig. 5a and b, respectively, are shown in Fig. 6. Because we focused on predicting the binding of the PICK1-PDZ to the PICK1-BAR domains, the linker region was excluded from the rmsd cluster analysis calculations. Representative conformations of the top three most populated clusters obtained in MREMD simulations, starting from the initial structures shown in Fig. 5a and b, respectively, are shown in Fig. 7a–c and d–f, respectively.

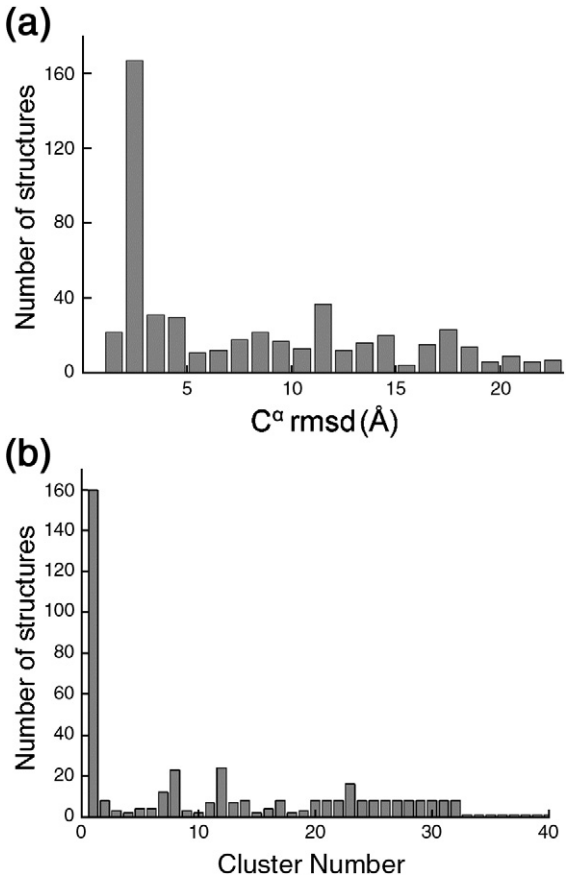

Fig. 6. Number of conformations of the PICK1 dual-BAR construct in clusters corresponding to the results of simulations started from (a) the structure shown in Fig. 5a, and (b) the structure shown in Fig. 5b. The cluster number (*x*-axis) has no relationship to the unknown C^{α} rmsd.

Remarkably, the representative structures of the two largest clusters in both MREMD simulations are nearly the same in spite of the large difference in starting point. In the most populated clusters (Fig. 7a and d), the PICK1-PDZ domain is bound to the center of the BAR dimer, and the position in which PDZ binds to the PICK1-BAR domain is almost the same as in the homology-modeled structure (Fig. 1).[43] However, the energy-based analysis also yields a binding mode of PICK1-PDZ to PICK1-BAR that is different from that predicted by Han and Weinstein.[43] In the second populated clusters (Fig. 7b and e), the PICK1-PDZ domain is bound closer to the N-terminus of the BAR domain, which is connected directly to the PDZ domain. The third populated cluster in each MREMD simulation of PICK1 (Fig. 7c and f) exhibits a different binding pattern in the two independent MREMD simulations, starting from the structures shown in Fig. 5a and b, respectively. In Fig. 6a, there are three clusters, numbers 8, 13 and 17, each containing 24 structures. Because the PDZ domain in clusters 8 and 17 binds to a similar position, as shown in Fig. 7b, the representative structure of cluster 13 was treated as the third largest cluster starting from the initial structure shown in Fig. 5a. Thus, the third cluster (Fig. 7c) obtained in simulations started from the initial structure illustrated in Fig. 5a is similar in the relative PDZ-BAR position to the largest one (Fig. 7a), but with the PDZ domain rotated by 180°. Both the binding position and the binding pattern of the structure shown in Fig. 7c are similar to those reported by Han and Weinstein (note, however, that this structure did not appear in the MREMD simulation starting from the structure shown in Fig. 5b, which yielded a position closer to the far edge of the crescent).[43]

Linker region of PICK1

The cluster analysis of the 40-residue linker segment of the PICK1 dual-BAR construct did not reveal any large linker cluster at the 3 Å rmsd cut-off; even the increase of the cut-off to 4 Å resulted in only two very small clusters. These results indicate that the linker region is flexible and does not adopt any dominant characteristic conformation.

Exploring the pathway of PDZ binding to the BAR dimer with MD simulations

To determine how the PDZ domain moves from a position remote from the convex face of the BAR dimer to the binding position, we carried out a series of short canonical MD simulations (a total of 64 trajectories) starting from the initial structure shown in Fig. 5b at 350 K. No simulation was attempted

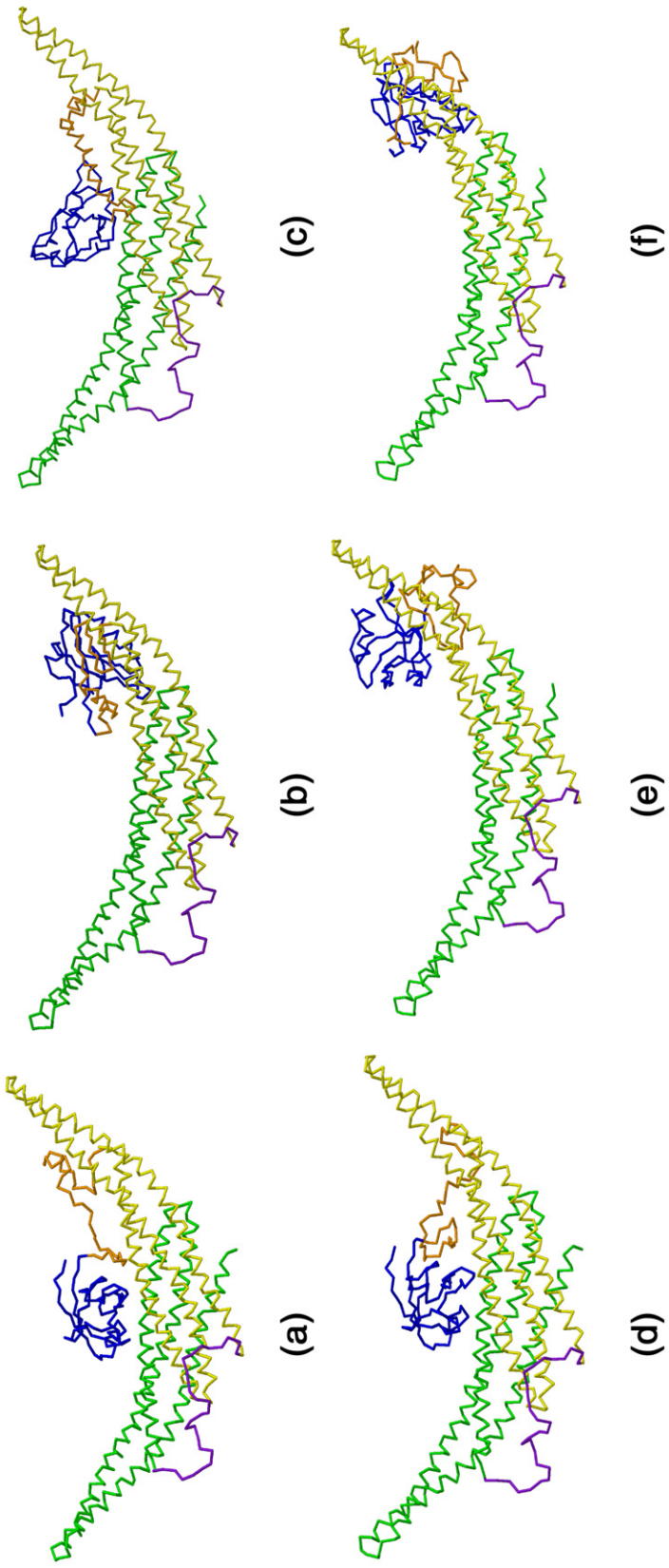

Fig. 7. Representative structures for the three top clusters from the UNRES/MREMD simulations with different initial starting structures of Fig. 5a (a – c) and Fig. 5b (d – f), respectively.

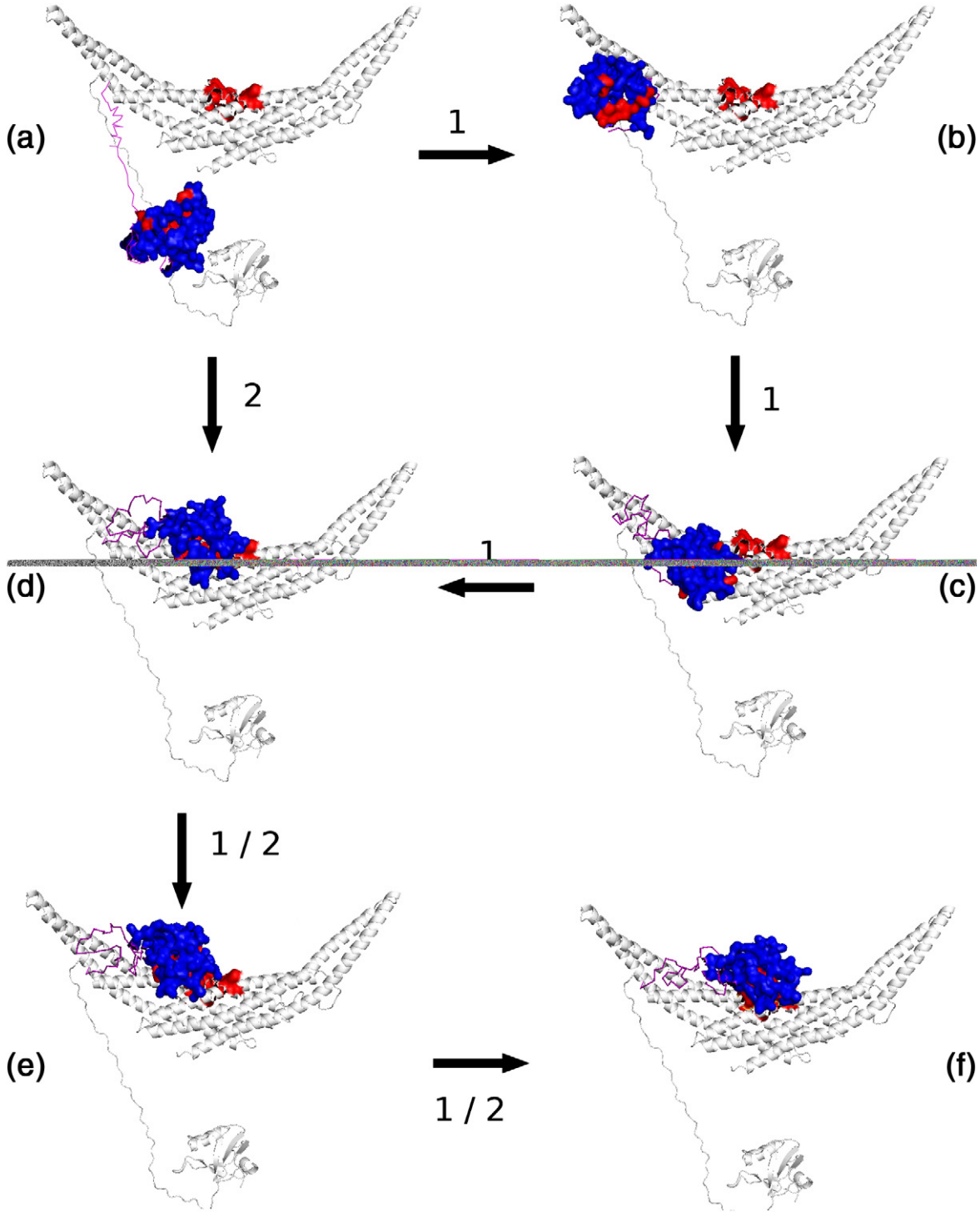

Fig. 8. Snapshots corresponding to two types of trajectories for binding the PICK1-PDZ domain to the dual-BAR domain, starting from the initial structure in which the PICK1-PDZ domain faces the convex surface of the PICK1-BAR dimer as shown in Fig. 5b. The initial structure of the PICK1 dual-BAR construct is colored light gray and shown in cartoon representation as a background to compare with the snapshots from the folding trajectory. The PDZ domain is shown as a surface view and is colored blue. The 40 residue linker region is colored purple. The interaction surfaces (i.e., the interface in the final complex) of both the PICK1-PDZ and PICK1-BAR domains are shown as a surface view and colored red. These structures were drawn with PYMOL (www.pymol.org). The two binding pathways are marked by arrows with 1 or 2 (or both if the conformations are similar in the two pathways).

with the initial structure shown in Fig. 5a because the PDZ domain prefers to bind to the concave face in both the MREMD simulation of the dual-BAR construct of PICK1 and the homology-modeled structure of PICK1,[43] and the initial position of the PDZ domain of the PICK1 structure in Fig. 5a might have a bias toward the concave cavity of the BAR domains of PICK1. Each trajectory was run for 3×10^6 steps (14.7 ps). Figure 8 shows the two observed pathways, drawn with PyMOL and marked 1 and 2 in the figure, that were found to lead to the binding of the PDZ domain to the center of the concave surface of the BAR-domain dimer.

Pathway 1. PDZ binds initially to the N-terminus of the BAR domain (Fig. 8b) and there is no direct hydrophobic interaction between the PDZ and the BAR domain (i.e., all nonpolar residues of the PDZ domains are >8.0 Å from those of the BAR domain). Rather, the stabilization comes from hydrophobic interactions between the linker region and the PDZ/BAR domains; note that the surface of PDZ that eventually interacts directly with the BAR dimer seen in the final model (Fig. 8f) of the complex (identified in red in the surface view) is pointing away from the BAR domain at this stage. The linker region is very flexible and the structure shown in Fig. 8b is not stable. The PDZ domain soon moves away from this metastable state towards the concave surface of the BAR-dimer domain (Fig. 8c) where it forms more hydrophobic contacts (Cys28/Leu140 and Val68/Phe400). Figure 8d – f show the subsequent repositioning of the PDZ domain towards the central binding pocket on the concave surface of the BAR dimer.

Pathway 2. In the second binding mode (path 2), the system bypasses the initial binding to the N-terminal part of the BAR domain seen in Fig. 8b and c, and the PDZ domain reaches the concave surface of the BAR-domain dimer directly (Fig. 8d); then, from the structure shown in Fig. 8d, the pathway goes through the position in Fig. 8e to that shown in Fig. 8f.

The characteristics of the two types of binding trajectories identified above for the interaction between the PICK1-PDZ domain and the PICK1-BAR-domain dimer suggest that the central binding pocket ultimately stabilizes the PDZ domain shown in Fig. 8f through favorable hydrophobic interactions involving residue pairs Leu16/Phe386, Ile21/Leu158, Val34/Leu158 and Val68/Phe161. The pathways, however, show that the interactions of the linker are significant at several putative intermediate positions of the PDZ domain. The specific role of the linker in the structural dynamics of PICK1 is unclear, however, and must be elucidated in the context of neighboring lipids because, in some analogous systems containing BAR domains (e.g., endophilin) the linker region has been suggested to play an active role in the interactions with the cell membrane and thereby affect the BAR domain interactions.[71]

Interactions that drive the binding of PDZ to the BAR dimer

Our results for the mode of stabilization of PDZ in the concave region of the BAR dimer suggest a key role for hydrophobic interactions. Notably, the cognate BAR dimers of SN9 and Arfaptin[37,64] also have large nonpolar patches in this concave region corresponding to the PDZ binding locus identified here. To learn more about the role of hydrophobic interactions in the binding process, the number of contacts between the nonpolar residues of the PDZ domain and those of the BAR domain were monitored during the simulation. Two residues were considered to be in hydrophobic contact if the distance between their side chains was <7.0 Å (for GLY, the distance between C^{α} atoms was used). Residues were assigned as nonpolar following the classification described in our earlier work.[72] The variation of the number of hydrophobic contacts with snapshot number is plotted in Fig. 9, where it can be seen that the number of hydrophobic contacts increases as the simulation progresses and reaches the highest values after approximately 230 snapshots (11.2 ps). The increase in number of hydrophobic contacts corresponds to the binding of the PDZ domain to the hydrophobic pocket of the BAR dimer.

A detailed set of hydrophobic interactions, corresponding to the structures shown in Fig. 8, is shown in Table 1, where it can be seen that the number of hydrophobic interactions increases as

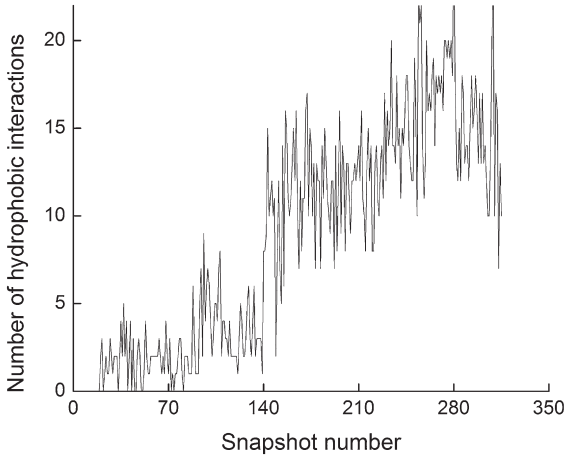

Fig. 9. Number of hydrophobic contacts between the PDZ and BAR domains of PICK1 during simulated binding.

Table 1. Hydrophobic contact map of structures shown in Fig. 8

Figure part	No. HBC[a]	Contact pairs[b]	
a	0	None	
b	0	None	
c	6	Gly24 / Gly404	Gly24 / Val405
		Cys28 / Leu140	Val68 / Phe400
		Val68 / Ile403	Val68 / Gly404
d	11	Leu16 / His393	Leu16 / Phe396
		Leu16 / Gly397	Tyr27 / Leu146
		Val34 / Tyr147	Val36 / Phe400
		Phe37 / Gly397	Phe37 / Phe400
		Val68 / Leu157	Val68 / Leu158
		Val68 / Phe161	
e	14	Leu16 / Gly397	Leu16 / Phe400
		Gly22 / Tyr147	Gly22 / Met150
		Gly23 / Tyr147	Gly23 / Met150
		Tyr32 / Tyr147	Tyr32 / Met150
		Val34 / Tyr147	Val34 / Met150
		Phe37 / Phe400	Val68 / Leu157
		Val68 / Leu158	Val68 / Phe161
f	16	Leu16 / Phe386	Leu16 / His393
		Gly18 / His393	Ile19 / His393
		Ile21 / Leu158	Ile21 / Tyr162
		Gly22 / Leu158	Gly23 / Leu158
		Gly24 / Phe161	Tyr27 / His153
		Val34 / Leu158	Phe37 / His393
		Phe37 / Phe396	Val68 / Phe161
		Val68 / Leu164	Ile74 / Phe386

[a] HBC, hydrophobic contacts.
[b] In the contact pairs, the residues on the left side of the forward slash are in the PDZ domain, and the residues on the right side of the forward slash are in the BAR domain.

binding proceeds. By comparing the hydrophobic contact pairs during the whole binding process, shown in Table 1, it can be seen that Leu16 and Val68 in the PDZ domain each form more than one contact with the BAR domain. Therefore, these two residues are important in driving the binding of the PDZ domain to the BAR domains. Because the PDZ domain moves a long way to the final binding position on the BAR domain, many nonpolar residues in the BAR domain contribute to this process. Also (shown only partially in Table 1f), residues Leu16, Ile21, Gly22, Val34 and Val68 in the PDZ domain and residues Leu158, Phe161, Tyr162, Phe386 of the PICK1 dual-BAR construct (corresponding to Phe161 on chain B) and His393 (corresponding to His168 on chain B) in the BAR domain are possibly important residues that stabilize the PDZ and BAR domain binding. The BAR-domain binding site for the PDZ domain is the most hydrophobic region of the BAR of PICK1; it is also in the BAR domains of SN9 and Arfaptin.

Discussion

The initial test of the UNRES-based simulations demonstrated that the protocol that we applied, based on the use of the UNRES potential, is able to reproduce native binding in SN9 in which the structure of the PX domain bound to the BAR dimer is known. Applying the same protocol to the analysis of domain interactions in PICK1, MREMD simulations with UNRES identified two possible binding modes of the PDZ domain to the BAR-domain dimer. The first is located in the center of the concave cavity of the crescent-shaped BAR dimer, whereas the second is near the N-terminus of the PICK1-BAR domain that connects directly to the PICK1-PDZ domain. Hydrophobic interactions were found to be the dominant stabilization forces, with the large convex face of the BAR dimer serving as a "net" to "catch" the PDZ domain, which then slides to the central binding pocket where it forms the most favorable hydrophobic interactions. The preferred binding site on the BAR domain is similar to that found by Han and Weinstein,[43] based on the Zdock,[73] PatchDock[74] and Rosetta Dock[75] homology-modeling protocols. Experimental observations suggested that the PICK1-PDZ domain inhibits the activity of the PICK1-BAR domain, and this auto-inhibition can be released by PICK1-PDZ ligand binding.[34,40] Our simulation results clearly show that the PICK1-PDZ domain prefers to bind to the concave region of the PICK1 BAR-dimer, which makes this site inaccessible to the interaction with membrane surfaces required for the common BAR dimer function.

The form of the final structure of the modified PICK1 is similar to that observed in Rac and Arfaptin binding.[37] This observation suggests that occupation of the concave region of the BAR dimer is a very likely basis for auto-inhibition of the BAR domain in experimental observations, consistent with the earlier model.[43] The other modes of binding obtained from the present work may arise from the fact that Han and Weinstein considered the PICK1 dimer that includes two PICK1-PDZ domains and studied the binding of a PDZ dimer to the BAR-domain dimer, whereas here we considered the binding of only a single PDZ domain. We note, however, that the alternative binding position of PDZ interacting with the BAR dimer identified here is near the N-terminus of the BAR domain, a region that has been shown to be essential for perturbing the membrane so as to facilitate the sensing and binding of curved membrane sections by BAR dimers.[42,76] Therefore, this alternative position is consistent with an inhibition of BAR–membrane interaction. Experimental evidence suggested that the auto-inhibition was released by PICK1-PDZ binding of ligands[44] and/or proximity to the membrane.[44]

We plan to extend the present study to the full PICK1 dimer (containing two PDZ domains) and evaluate the changes produced by PDZ-ligand binding as soon as the fine-grained version of UNRES to treat multichain proteins becomes available.

Materials and Methods

The UNRES force field

In the UNRES model, a polypeptide chain is represented by a sequence of α-carbon atoms connected by virtual bonds with attached side chains.[45–63] Two interaction sites are used to represent each amino acid, one located in the middle between two consecutive C^{α} atoms and the other one at the center of mass of the corresponding side chain. The C^{α} atoms serve only to define the geometry. UNRES is a physics-based force field that has been carefully derived as a restricted free energy function of an all-atom polypeptide chain plus the surrounding water.[45] The all-atom energy is averaged over the degrees of freedom that are lost when passing from the all-atom to the simplified representation. The restricted free energy is further decomposed into factors representing the interactions within and between a given number of united interaction sites. Expansion of these factors into a Kubo generalized cumulant series[65] made it possible to obtain approximate analytical expressions for the respective terms, including the multibody terms, which are derived in other force fields from structural databases or on a heuristic basis.[77] The details of the theoretical basis are described elsewhere.[49] The energy function of the virtual-bond chain is expressed as:

$$\begin{aligned} U(X,T) = {} & w_{sc}\sum_{i<j} U_{sc_i sc_j}(X) + w_{scp}\sum_{i\neq j} U_{sc_i p_j}(X) \\ & + w_{pp}^{VDW}\sum_{i<j-1} U_{p_i p_j}^{VDW}(X) + w_{pp}^{el} f_2(T)\sum_{i<j-1} U_{p_i p_j}^{el}(X) \\ & + w_{tor} f_2(T)\sum i U_{tor}(\gamma_i) + w_{tord} f_3(T)\sum i U_{tord}(\gamma_i,\gamma_{i+1}) \\ & + w_b\sum_i U_b(\theta_i) + w_{rot}\sum_i U_{rot}(\alpha_{sc_i},\beta_{sc_i}) \\ & + w_{corr}^{(3)} f_3(T) U_{corr}^{(3)}(X) + w_{corr}^{(4)} f_4(T) U_{corr}^{(4)}(X) \\ & + w_{corr}^{(5)} f_5(T) U_{corr}^{(5)}(X) + w_{corr}^{(6)} f_6(T) U_{corr}^{(6)}(X) \\ & + w_{turn}^{(3)} f_3(T) U_{turn}^{(3)}(X) + w_{turn}^{(4)} f_4(T) U_{turn}^{(4)}(X) \\ & + w_{turn}^{(6)} f_6(T) U_{turn}^{(6)}(X) + w_{bond}\sum_i U_{bond}(d_i) \end{aligned} \quad (1)$$

where X represents the set of coordinates of a conformation of the coarse-grained chain and T is absolute temperature. The terms $U_{sc_i sc_j}(X)$ are the potentials of mean force of the interaction of isolated side chains in water (with the contribution from the solvent already included). The terms $U_{sc_i p_j}(X)$ are the excluded-volume potentials of interactions between side chains and peptide groups. The terms $U_{p_i p_j}^{VDW}(X)$ are the Lennard-Jones potentials and $U_{p_i p_j}^{el}(X)$ are the averaged electrostatic-interaction potentials between peptide groups. The terms $U_{tor}(\gamma_i)$ and $U_{tord}(\gamma_i,\gamma_{i+1})$ are the virtual-bond torsional and double-torsional potentials, respectively. The terms $U_b(\theta_i)$, $U_{rot}(\alpha_{sc_i},\beta_{sc_i})$, and $U_{bond}(d_i)$ denote the energy of virtual-bond angle bending, side-chain rotamers, and virtual-bond stretching, respectively. The terms $U_{corr}^{(m)}$ represent the correlation or multibody contribution from the backbone-local and backbone-electrostatic interactions. The terms $U_{turn}^{(m)}$ denote the correlation contribution involving m consecutive peptide groups. The energy-term weights corresponding to second-order and higher-order generalized cumulants are multiplied by the appropriate scaling factor, $f_n(T)$, defined in Eq. (2), where n is the order of a cumulant-based term:[49]

$$f_n(T) = \frac{1n[\exp(1)+\exp(1)]}{1n\left\{\exp\left[\left(\frac{T}{T_0}\right)^{n-1}\right]+\exp\left[\left(\frac{T}{T_0}\right)^{n-1}\right]\right\}} \quad (2)$$

T_0 is the arbitrary reference temperature (we set T_0 as 300 K), and T is the current temperature. The force field used in this work was developed by global search of the energy-term weights.[62]

Generating initial structures

Sorting Nexin 9

To take advantage of massively parallel computations to run simulations in real time, we used the recently developed fine-grained UNRES code[63] that has not yet been extended to treat multi-chain proteins. Preliminary UNRES/MD simulations of the SN9 monomer, extracted as chain A from the X-ray structure[64] of the dimer (data not shown) demonstrated that, in this monomer, PX binds to the side of the BAR domain (bottom side of the yellow-BAR domain in Fig. 2a) that normally contacts the BAR domain of chain B of the native dimer. Therefore, two BAR domains bound as in the native dimer were used to compute the binding between the PX and BAR domains. In order to make use of the (currently) single-chain UNRES code in this simulation, a single chain was constructed containing two BAR domains and one PX domain, based on the experimental structure of SN9, as shown in Fig. 2b. To this end, the PX domain from chain B of the dimer (colored light gray in Fig. 2a) was removed, and then the linker that connects the BAR and PX domains of chain B (colored purple in Fig. 2a) in the native dimer, was used to connect the BAR domain of chain B to that of chain A (colored yellow in Fig. 2a) to form a single chain. This artificial construct, which contains two monomeric BAR domains and one PX domain, is referred to here as a dual-BAR monomer of SN9 (Fig. 2b). Although the two BAR domains were

Fig. 10. The process of generating the structure of the PICK1 dual-BAR construct from the PICK1 dimer structure predicted by Han and Weinstein.[43] (a) The gray PDZ domain (in the black circle) was removed from its position in Fig. 1. (b) The purple linker region of chain B was artificially joined to the C-terminus of the BAR domain of chain A (colored yellow) with Modeller.[66–69] The two small black circles with a black arrow between them indicate the positions of the A and B chains, respectively, that are superposed to join the A and B chains as shown in (c).

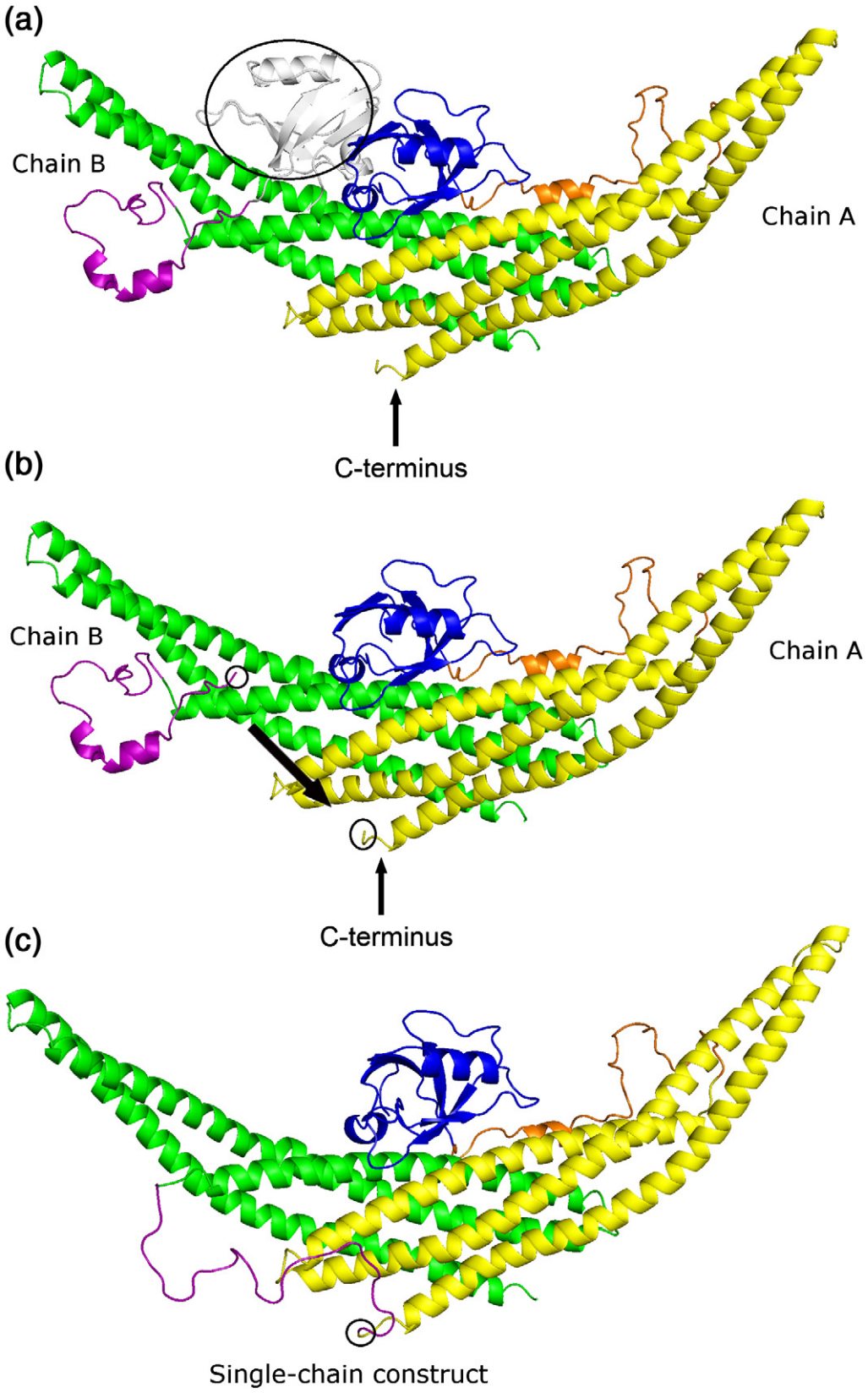

Fig. 10 (*legend on previous page*)

artificially connected, their arrangement was maintained as in the experimental structure, so that the dual-BAR "monomer" of SN9 is very similar to the SN9 dimer except that it lacks one of the PX domains. Comparison of Fig. 2a and b shows that a second PX domain (colored light gray) is too distant from the PX–BAR complex to affect the interaction, making the dual-BAR monomer of SN9 suitable for the test simulations.

For the test simulations, the PX domain was separated from the BAR domain as far as the length of the covalent linker between it and the BAR domain of the chain would allow, and was placed above the BAR domains of the dual-BAR monomer of SN9, as shown in Fig. 3. It should be noted that the linker between the PX and BAR domain consists of only 13 residues (167–179) in SN9 whereas the linker between the PDZ and BAR domains in PICK1 consists of 40 residues. Therefore, in order to test the binding simulation power of UNRES for domains connected by a 40 residue linker, the linker region of SN9 was extended by sequestering an additional 12 residues (155–166) from the SN9 PX domain and 15 residues (180–194) from the BAR domain, and assigned them to the linker region as shown in Fig. 6. In this way, an initial structure of the SN9 dual-BAR construct with a 40 residue linker (colored orange) was built as shown in Fig. 3.

PICK1

The protocol described above was applied to PICK1. The experimental structure of the PICK1 dimer is not available, so the homology-modeled structure of the PICK1-BAR dimer was used.[43] As was done for SN9, the PDZ domain (colored gray in Fig. 10a) was removed, the linker (colored purple) was then connected to the C-terminus of chain A of the homology-modeled structure of PICK1, and the BAR domains were kept in the same arrangement as in the homology-modeled structure (Fig. 10b). This artificial construct thus contains two monomeric BAR domains and a PDZ domain, and is referred to here as a dual-BAR monomer of PICK1 (shown in Fig. 10c). The 40 residue linker of PICK1 is long enough to provide sufficient mobility to pull the PDZ domain away from the two artificially connected BAR domains. Two initial structures were therefore generated for PICK1, as shown in Fig. 5. In these two initial structures, the PICK1-PDZ domain is located on opposite sides, away from the PICK1-BAR domains. The initial shape of the 40 residue linker (colored orange in Fig. 5) between the PDZ and the BAR dimer was built with Modeller.[66–69]

Simulation details

During the simulations, C^{α}-distance harmonic restraints were applied to the structures of the SN9-PX, PICK1-PDZ and dual-BAR domains with a force constant of 50.0 kcal/(mol Å^2). However, there was no restraint between domains, and the linker between the two domains was free to move and change conformation.

MREMD simulation details

To sample the conformational space and location of the binding sites for both proteins, MREMD simulations were carried out for both SN9 and PICK1. All MREMD simulations were run at 16 temperatures (210, 230, 250, 270, 280, 290, 300, 310, 320, 340, 360, 380, 400, 420, 440 and 460 K). In our earlier work,[61] we found that this temperature range enables a protein to explore the conformational space efficiently. Four trajectories per temperature were run (a total of 64 trajectories), and replica exchange was done after every 2×10^4 MD steps.

MD simulation details

Canonical MD simulations were also done for PICK1 to explore how the PDZ domain moves from a remote starting position to the most favorable binding sites on the BAR domains of PICK1. In earlier work,[62] when the force field was parameterized, a folding temperature of 300 K was found for this force field for the tryptophan cage (trp-cage) and the tryptophan zipper 2 (trpzip2). Since PICK1 is much larger than these two proteins, it presumably has a higher folding transition temperature. On the other hand, in order to accelerate the simulation, 350 K (the presumed folding temperature) was used for canonical MD simulation of the PICK1 dual-BAR construct shown in Fig. 5b. The Berendsen thermostat, implemented in UNRES/MD in our earlier work,[57] was used to maintain constant temperature; the coupling constant τ was 0.489 fs, which was used in our earlier work to provide a compromise between the extent of fluctuations of the potential and kinetic energy. The time increment for integrating the equations of motion δt was 4.89 fs.

Acknowledgements

This work was supported by grants from the U.S. National Institutes of Health (R01 GM-14312 and P01 DA-012408) and the U.S. National Science Foundation (MCB05-41633), and by grant DS/8372-4-0-138-10 from the Polish Ministry of Science and Higher Education. The research used computational resources from (a) the 736-processor Beowulf cluster at the Baker Laboratory of Chemistry and Chemical Biology, Cornell University, (b) the National Science Foundation Terascale Computing System at the Pittsburgh Supercomputer Center, (c) the John von Neumann Institute for Computing at the Central Institute for Applied Mathematics, Forschungszentrum Julich, Germany, (d) the Beowulf cluster at the Department of Computer Science, Cornell University, (e) the Center for Computation and Technology at Louisiana State University, which is supported by funding from the Louisiana legislature, (f) the 45-processor Beowulf cluster at the Faculty of Chemistry, University of Gdańsk, (g) the Informatics Center of the Metropolitan Academic Network (IC MAN) in Gdańsk, and (h) the Interdisciplinary Center of Mathematical and Computer Modeling (ICM) at the University of Warsaw.

References

1. Staudinger, J., Zhou, J., Burgess, R., Elledge, S. J. & Olson, E. N. (1995). PICK1: a perinuclear binding protein and substrate for protein kinase C isolated by the yeast two-hybrid system. *J. Cell Biol.* **128**, 263–271.
2. Sheng, M. & Sala, C. (2001). PDZ domains and the organization of supramolecular complexes. *Annu. Rev. Neurosci.* **24**, 1–29.
3. Hung, A. Y. & Sheng, M. (2002). PDZ domains: structural modules for protein complex assembly. *J. Biol. Chem.* **277**, 5699–5702.
4. Takei, K., Slepnev, V. I., Haucke, V. & De Camilli, P. (1999). Functional partnership between amphiphysin and dynamin in clathrin-mediated endocytosis. *Nat. Cell Biol.* **1**, 33–39.
5. Staudinger, J., Lu, J. & Olson, E. N. (1997). Specific interaction of the PDZ domain protein PICK1 with the COOH terminus of protein kinase Cα. *J. Biol. Chem.* **272**, 32019–32024.
6. Torres, R., Firestein, B. L., Dong, H., Staudinger, J., Olson, E. N., Huganir, R. L. *et al.* (1998). PDZ proteins bind, cluster, and synaptically colocalize with Eph receptors and their ephrin ligands. *Neuron*, **21**, 1453–1463.
7. Dev, K. K., Nishimune, A., Henley, J. M. & Nakanishi, S. (1999). The protein kinase Cα binding protein PICK1 interacts with short but not long form alternative splice variants of AMPA receptor subunits. *Neuropharmacology*, **38**, 635–644.
8. Takeya, R., Takeshige, K. & Sumimoto, H. (2000). Interaction of the PDZ domain of human PICK1 with class I ADP-ribosylation factors. *Biochem. Biophys. Res. Commun.* **267**, 149–155.
9. Boudin, H., Doan, A., Xia, J., Shigemoto, R., Huganir, R. L., Worley, P. & Craig, A. M. (2000). Presynaptic clustering of mGluR7a requires the PICK1 PDZ domain binding site. *Neuron*, **28**, 485–497.
10. El Far, O., Airas, J., Wischmeyer, E., Nehring, R. B., Karschin, A. & Betz, H. (2000). Interaction of the C-terminal tail region of the metabotropic glutamate receptor 7 with the protein kinase C substrate PICK1. *Eur. J. Neurosci.* **12**, 4215–4221.
11. Cowan, C. A., Yokoyama, N., Bianchi, L. M., Henkemeyer, M. & Fritzsch, B. (2000). EphB2 guides axons at the midline and is necessary for normal vestibular function. *Neuron*, **26**, 417–430.
12. Lin, W. J., Chang, Y. F., Wang, W. L. & Huang, C. Y. (2001). Mitogen-stimulated TIS21 protein interacts with a protein-kinase-Cα-binding protein rPICK1. *Biochem. J.* **354**, 635–643.
13. Lin, S. H., Arai, A. C., Wang, Z., Nothacker, H. P. & Civelli, O. (2001). The carboxyl terminus of the prolactin-releasing peptide receptor interacts with PDZ domain proteins involved in α-amino-3-hydroxy-5-methylisoxazole-4-propionic acid receptor clustering. *Mol. Pharmacol.* **60**, 916–923.
14. Torres, G. E., Yao, W. D., Mohn, A. R., Quan, H., Kim, K. M., Levey, A. I. *et al.* (2001). Functional interaction between monoamine plasma membrane transporters and the synaptic PDZ domain-containing protein PICK1. *Neuron*, **30**, 121–134.
15. Penzes, P., Johnson, R. C., Sattler, R., Zhang, X., Huganir, R. L., Kambampati, V. *et al.* (2001). The neuronal Rho-GEF Kalirin-7 interacts with PDZ domain-containing proteins and regulates dendritic morphogenesis. *Neuron*, **29**, 229–242.
16. Jaulin-Bastard, F., Saito, H., Le Bivic, A., Ollendorff, V., Marchetto, S., Birnbaum, D. & Borg, J. P (2001). The ERBB2/HER2 receptor differentially interacts with ERBIN and PICK1 PSD-95/DLG/ZO-1 domain proteins. *J. Biol. Chem.* **276**, 15256–15263.
17. Perroy, J., El Far, O., Bertaso, F., Pin, J. P., Betz, H., Bockaert, J. & Fagni, L (2002). PICK1 is required for the control of synaptic transmission by the metabotropic glutamate receptor 7. *EMBO J.* **21**, 2990–2999.
18. Duggan, A., Garcia-Anoveros, J. & Corey, D. P (2002). The PDZ domain protein PICK1 and the sodium channel BNaC1 interact and localize at mechanosensory terminals of dorsal root ganglion neurons and dendrites of central neurons. *J. Biol. Chem.* **277**, 5203–5208.
19. Hruska-Hageman, A. M., Wemmie, J. A., Price, M. P. & Welsh, M. J. (2002). Interaction of the synaptic protein PICK1 (protein interacting with C kinase 1) with the non-voltage gated sodium channels BNC1 (brain Na+ channel 1) and ASIC (acid-sensing ion channel). *Biochem. J.* **361**, 443–450.
20. Williams, M. E., Wu, S. C., McKenna, W. L. & Hinck, L. (2003). Surface expression of the netrin receptor UNC5H1 is regulated through a protein kinase C-interacting protein/protein kinase-dependent mechanism. *J. Neurosci.* **23**, 11279–11288.
21. Enz, R. & Croci, C. (2003). Different binding motifs in metabotropic glutamate receptor type 7b for filamin A, protein phosphatase 1C, protein interacting with protein kinase C (PICK) 1 and syntenin allow the formation of multimeric protein complexes. *Biochem. J.* **372**, 183–191.
22. Leonard, A. S., Yermolaieva, O., Hruska-Hageman, A., Askwith, C. C., Price, M. P., Wemmie, J. A. & Welsh, M. J. (2003). cAMP-dependent protein kinase phosphorylation of the acid-sensing ion channel-1 regulates its binding to the protein interacting with C-kinase-1. *Proc. Natl Acad. Sci. USA*, **100**, 2029–2034.
23. Hirbec, H., Francis, J. C., Lauri, S. E., Braithwaite, S. P., Coussen, F., Mulle, C. *et al.* (2003). Rapid and differential regulation of AMPA and kainate receptors at hippocampal mossy fibre synapses by PICK1 and GRIP. *Neuron*, **37**, 625–638.
24. Meyer, G., Varoqueaux, F., Neeb, A., Oschlies, M. & Brose, N. (2004). The complexity of PDZ domain-mediated interactions at glutamatergic synapses: a case study on neuroligin. *Neuropharmacology*, **47**, 724–733.
25. Excoffon, K. J., Hruska-Hageman, A., Klotz, M., Traver, G. L. & Zabner, J. (2004). A role for the PDZ-binding domain of the coxsackie B virus and adenovirus receptor (CAR) in cell adhesion and growth. *J. Cell. Sci.* **117**, 4401–4409.
26. Reymond, N., Garrido-Urbani, S., Borg, J. P., Dubreuil, P. & Lopez, M. (2005). PICK-1: a scaffold protein that interacts with Nectins and JAMs at cell junctions. *FEBS Lett.* **579**, 2243–2249.
27. Xia, J., Chung, H. J., Wihler, C., Huganir, R. L. & Linden, D. J. (2000). Cerebellar long-term depression requires PKC-regulated interactions between GluR2/3 and PDZ domain-containing proteins. *Neuron*, **28**, 499–510.

28. Daw, M. I., Chittajallu, R., Bortolotto, Z. A., Dev, K. K., Duprat, F., Henley, J. M. *et al.* (2000). PDZ proteins interacting with C-terminal GluR2/3 are involved in a PKC-dependent regulation of AMPA receptors at hippocampal synapses. *Neuron*, **28**, 873–886.
29. Jansen, A. M., Nassel, D. R., Madsen, K. L., Jung, A. G., Gether, U. & Kjaerulff, O. (2009). PICK1 expression in the Drosophila central nervous system primarily occurs in the neuroendocrine system. *J. Comp. Neurol.* **517**, 313–332.
30. Xia, J., Zhang, X., Staudinger, J. & Huganir, R. L. (1999). Clustering of AMPA receptors by the synaptic PDZ domain-containing protein PICK1. *Neuron*, **22**, 179–187.
31. Gardner, S. M., Takamiya, K., Xia, J., Suh, J. G., Johnson, R., Yu, S. & Huganir, R. L. (2005). Calcium-permeable AMPA receptor plasticity is mediated by subunit-specific interactions with PICK1 and NSF. *Neuron*, **45**, 903–915.
32. Hanley, J. G. & Henley, J. M. (2005). PICK1 is a calcium-sensor for NMDA-induced AMPA receptor trafficking. *EMBO J.* **24**, 3266–3278.
33. Dev, K. K., Nakajima, Y., Kitano, J., Braithwaite, S. P., Henley, J. M. & Nakanishi, S. (2000). PICK1 interacts with and regulates PKC phosphorylation of mGLUR7. *J. Neurosci.* **20**, 7252–7257.
34. Perez, J. L., Khatri, L., Chang, C., Srivastava, S., Osten, P. & Ziff, E. B. (2001). PICK1 targets activated protein kinase Cα to AMPA receptor clusters in spines of hippocampal neurons and reduces surface levels of the AMPA-type glutamate receptor subunit 2. *J. Neurosci.* **21**, 5417–5428.
35. Baron, A., Deval, E., Salinas, M., Lingueglia, E., Voilley, N. & Lazdunski, M. (2002). Protein kinase C stimulates the acid-sensing ion channel ASIC2a via the PDZ domain-containing protein PICK1. *J. Biol. Chem.* **277**, 50463–50468.
36. Elkins, J. M., Papagrigoriou, E., Berridge, G., Yang, X., Phillips, C., Gileadi, C. *et al.* (2007). Structure of PICK1 and other PDZ domains obtained with the help of self-binding C-terminal extensions. *Protein Sci.* **16**, 683–694.
37. Tarricone, C., Xiao, B., Justin, N., Walker, P. A., Rittinger, K., Gamblin, S. J. & Smerdon, S. J. (2001). The structural basis of Arfaptin-mediated cross-talk between Rac and Arf signalling pathways. *Nature*, **411**, 215–219.
38. Masuda, M., Takeda, S., Sone, M., Ohki, T., Mori, H., Kamioka, Y. & Mochizuki, N. (2006). Endophilin BAR domain drives membrane curvature by two newly identified structure-based mechanisms. *EMBO J.* **25**, 2889–2897.
39. Peter, B. J., Kent, H. M., Mills, I. G., Vallis, Y., Butler, P. J., Evans, P. R. & McMahon, H. T. (2004). BAR domains as sensors of membrane curvature: the amphiphysin BAR structure. *Science*, **303**, 495–499.
40. Lu, W. & Ziff, E. B. (2005). PICK1 interacts with ABP/GRIP to regulate AMPA receptor trafficking. *Neuron*, **47**, 407–421.
41. Jin, W., Ge, W. P., Xu, J., Cao, M., Peng, L., Yung, W. *et al.* (2006). Lipid binding regulates synaptic targeting of PICK1, AMPA receptor trafficking, and synaptic plasticity. *J. Neurosci.* **26**, 2380–2390.
42. Khelashvili, G., Harries, D. & Weinstein, H. (2009). Modeling membrane deformations and lipid demixing upon protein-membrane interaction: the BAR dimer adsorption. *Biophys. J.* **97**, 1626–1635.
43. Han, D. S. & Weinstein, H. (2008). Auto-inhibition in the multi-domain protein PICK1 revealed by dynamic models of its quaternary structure. *Biophys. J.* **94**, 67–76.
44. Madsen, K. L., Eriksen, J., Milan-Lobo, L., Han, D. S., Niv, M. Y., Ammendrup-Johnsen, I. *et al.* (2008). Membrane localization is critical for activation of the PICK1 BAR domain. *Traffic*, **9**, 1327–1343.
45. Liwo, A., Oldziej, S., Pincus, M. R., Wawak, R. J., Rackovsky, S. & Scheraga, H. A. (1997). A united-residue force field for off-lattice protein-structure simulations. I: Functional forms and parameters of long-range side-chain interaction potentials from protein crystal data. *J. Comput. Chem.* **18**, 849–873.
46. Liwo, A., Pincus, M. R., Wawak, R. J., Rackovsky, S., Oldziej, S. T. & Scheraga, H. A. (1997). A united-residue force field for off-lattice protein-structure simulations. II: Parameterization of local interactions and determination of the weights of energy terms by Z-score optimization. *J. Comput. Chem.* **18**, 874–887.
47. Liwo, A., Kazmierkiewicz, R., Czaplewski, C., Groth, M., Oldziej, S., Wawak, R. J. *et al.* (1998). A united-residue force field for off-lattice protein-structure simulations.III. Origin of backbone hydrogen-bonding cooperativity in united-residue potentials. *J. Comput. Chem.* **19**, 259–276.
48. Lee, J., Ripoll, D. R., Czaplewski, C., Pillardy, J., Wedemeyer, W. J. & Scheraga, H. A. (2001). Optimization of parameters in macromolecular potential energy functions by conformational space annealing. *J. Phys. Chem. B*, **105**, 7291–7298.
49. Liwo, A., Czaplewski, C., Pillardy, J. & Scheraga, H. A. (2001). Cumulant-based expressions for the multibody terms for the correlation between local and electrostatic interactions in the united-residue force field. *J. Chem. Phys.* **115**, 2323–2347.
50. Pillardy, J., Czaplewski, C., Liwo, A., Wedemeyer, W. J., Lee, J., Ripoll, D. R. *et al.* (2001). Development of physics-based energy functions that predict medium-resolution structures for proteins of the α, β, and α/β structural classes. *J. Phys. Chem. B*, **105**, 7299–7311.
51. Liwo, A., Arlukowicz, P., Czaplewski, C., Oldziej, S., Pillardy, J. & Scheraga, H. A. (2002). A method for optimizing potential-energy functions by a hierarchical design of the potential-energy landscape: application to the UNRES force field. *Proc. Natl Acad. Sci. USA*, **99**, 1937–1942.
52. Oldziej, S., Kozlowska, U., Liwo, A. & Scheraga, H. A. (2003). Determination of the potentials of mean force for rotation about C-C virtual bonds in polypeptides from the ab initio energy surfaces of terminally blocked glycine, alanine, and proline. *J. Phys. Chem. A*, **107**, 8035–8046.
53. Liwo, A., Oldziej, S., Czaplewski, C., Kozlowska, U. & Scheraga, H. A. (2004). Parametrization of backbone-electrostatic and multibody contributions to the UNRES force field for protein-structure prediction from ab initio energy surfaces of model systems. *J. Phys. Chem. B*, **108**, 9421–9438.

54. Liwo, A., Arlukowicz, P., Oldziej, S., Czaplewski, C., Makowski, M. & Scheraga, H. A. (2004). Optimization of the UNRES force field by hierarchical design of the potential-energy landscape. 1. Tests of the approach using simple lattice protein models. *J. Phys. Chem. B*, **108**, 16918–16933.
55. Oldziej, S., Liwo, A., Czaplewski, C., Pillardy, J. & Scheraga, H. A. (2004). Optimization of the UNRES force field by hierarchical design of the potential-energy landscape. 2. Off-lattice tests of the method with single proteins. *J. Phys. Chem. B*, **108**, 16934–16949.
56. Oldziej, S., Lagiewka, J., Liwo, A., Czaplewski, C., Chinchio, M., Nanias, M. & Scheraga, H. A. (2004). Optimization of the UNRES force field by hierarchical design of the potential-energy landscape. 3. Use of many proteins in optimization. *J. Phys. Chem. B*, **108**, 16950–16959.
57. Liwo, A., Khalili, M. & Scheraga, H. A. (2005). Ab initio simulations of protein-folding pathways by molecular dynamics with the united-residue model of polypeptide chains. *Proc. Natl Acad. Sci. USA*, **102**, 2362–2367.
58. Khalili, M., Liwo, A., Rakowski, F., Grochowski, P. & Scheraga, H. A. (2005). Molecular dynamics with the united-residue model of polypeptide chains. I. Lagrange equations of motion and tests of numerical stability in the microcanonical mode. *J. Phys. Chem. B*, **109**, 13785–13797.
59. Khalili, M., Liwo, A., Jagielska, A. & Scheraga, H. A. (2005). Molecular dynamics with the united-residue model of polypeptide chains. II. Langevin and Berendsen-bath dynamics and tests on model α-helical systems. *J. Phys. Chem. B*, **109**, 13798–13810.
60. Khalili, M., Liwo, A. & Scheraga, H. A. (2006). Kinetic studies of folding of the B-domain of staphylococcal protein A with molecular dynamics and a united-residue (UNRES) model of polypeptide chains. *J. Mol. Biol.* **355**, 536–547.
61. Liwo, A., Khalili, M., Czaplewski, C., Kalinowski, S., Oldziej, S., Wachucik, K. & Scheraga, H. A. (2007). Modification and optimization of the United-Residue (UNRES) potential energy function for canonical simulations. I. Temperature dependence of the effective energy function and tests of the optimization method with single training proteins. *J. Phys. Chem. B*, **111**, 260–285.
62. He, Y., Xiao, Y., Liwo, A. & Scheraga, H. A. (2009). Exploring the parameter space of the coarse-grained UNRES force field by random search: selecting a transferable medium-resolution force field. *J. Comput. Chem.* **30**, 2127–2135.
63. Liwo, A., Oldziej, S., Czaplewski, C., Kleinerman, D. S., Blood, P. & Scheraga, H. A. (2010). Implementation of molecular dynamics and its extensions with the coarse-grained UNRES force field on massively parallel systems; towards millisecond-scale simulations of protein structure, dynamics, and thermodynamics. *J. Chem. Theor. Comput.* **6**, 890–909.
64. Pylypenko, O., Lundmark, R., Rasmuson, E., Carlsson, S. R. & Rak, A. (2007). The PX-BAR membrane-remodeling unit of sorting nexin 9. *EMBO J.* **26**, 4788–4800.
65. Kubo, R. (1962). Generalized cumulant expansion method. *J. Phys. Soc. Jpn*, **17**, 1100.
66. Sali, A. & Blundell, T. L. (1993). Comparative protein modelling by satisfaction of spatial restraints. *J. Mol. Biol.* **234**, 779–815.
67. Fiser, A., Do, R. K. & Sali, A. (2000). Modeling of loops in protein structures. *Protein Sci.* **9**, 1753–1773.
68. Marti-Renom, M. A., Stuart, A. C., Fiser, A., Sanchez, R., Melo, F. & Sali, A. (2000). Comparative protein structure modeling of genes and genomes. *Annu. Rev. Biophys. Biomol. Struct.* **29**, 291–325.
69. Eswar, N., Webb, B., Marti-Renom, M. A., Madhusudhan, M. S., Eramian, D., Shen, M. Y. *et al.* (2006). Comparative protein structure modeling using Modeller. *Curr. Protoc. Bioinformatics*, John Wiley, chapt. 5, unit 5.6.
70. Gower, J. C. & Ross, G. J. S. (1969). Minimum spanning trees and single linkage cluster analysis. *J. R. Stat. Soc. C*, **18**, 54–64.
71. Hatzakis, N. S., Bhatia, V. K., Larsen, J., Madsen, K. L., Bolinger, P. Y., Kunding, A. H. *et al.* (2009). How curved membranes recruit amphipathic helices and protein anchoring motifs. *Nat. Chem. Biol.* **5**, 835–841.
72. Meirovitch, H., Rackovsky, S. & Scheraga, H. A. (1980). Empirical studies of hydrophobicity. 1. Effect of protein size on the hydrophobic behavior of amino acids. *Macromolecules*, **13**, 1398–1405.
73. Chen, R., Li, L. & Weng, Z. (2003). ZDOCK: an initial-stage protein-docking algorithm. *Proteins: Struct. Funct. Genet.* **52**, 80–87.
74. Schneidman-Duhovny, D., Inbar, Y., Polak, V., Shatsky, M., Halperin, I., Benyamini, H. *et al.* (2003). Taking geometry to its edge: fast unbound rigid (and hinge-bent) docking. *Proteins: Struct. Funct. Genet.* **52**, 107–112.
75. Gray, J. J., Moughon, S., Wang, C., Schueler-Furman, O., Kuhlman, B., Rohl, C. A. & Baker, D. (2003). Protein–protein docking with simultaneous optimization of rigid-body displacement and side-chain conformations. *J. Mol. Biol.* **331**, 281–299.
76. Bhatia, V. K., Madsen, K. L., Bolinger, P. Y., Kunding, A., Hedegard, P., Gether, U. & Stamou, D. (2009). Amphipathic motifs in BAR domains are essential for membrane curvature sensing. *EMBO J.* **28**, 3303–3314.
77. Kolinski, A. & Skolnick, J. (1992). Discretized model of proteins I. Monte-Carlo study of cooperativity in homopolypeptides. *J. Chem. Phys.* **97**, 9412–9426.